BENEFICIAL EFFECTS OF CONCRETE RELAXATION ON DISPLACEMENT-INDUCED COLUMN FORCES IN CONTINUOUS PRESTRESSED CONCRETE BRIDGES

Ebadollah Honarvar, PhD, Structural/Bridge Engineer, Jacobs, New York, NY
Sri Sritharan, PhD, Wilson Engineering Professor, Department of Civil, Construction, and Environmental Engineering, Iowa State University, Ames, IA
Matt Rouse, PhD, Senior Lecturer, Department of Civil, Construction, and Environmental Engineering, Iowa State University, Ames, IA

ABSTRACT

During and after construction, cast-in-place posttensioned concrete box-girder bridges (CIP/PCBB) experience continuous movement due to time-dependent shortening of the superstructure. As a result, displacement-induced forces are produced in the columns. These forces are currently overestimated due to neglect of the beneficial effects of concrete relaxation. In this paper, a combination of an experimental investigation and finite-element analysis (FEA) was employed to characterize the concrete relaxation and demonstrate its beneficial effects on the columns of a prototype CIP/PCBB.

Using a series of tests, this study first quantifies relaxation for normal strength concrete at different loading ages. It was found that relaxation resulted in a significant reduction in the displacement-induced forces for all the tests under the state of constant strain. Based on the test results, relaxation functions were established and compared to the analytical models to determine suitable models for relaxation. Then, time-dependent deformations and stresses from the time of construction to the completion of a demonstrative CIP/PCBB with due consideration to concrete relaxation were calculated using the FEA. It was found that relaxation can reduce the displacement-induced forces in the columns by as much as 53%.

Keywords: Creep, Relaxation, Shrinkage, Posttensioned concrete box-girder bridge, Finite-element analysis, Displacement-induced column forces

INTRODUCTION

During and after construction, time-dependent displacement-induced forces are developed in the columns of cast-in-place posttensioned concrete box-girder bridges (CIP/PCBB) due to shortening of superstructure, as shown in Fig. 1. The magnitude of these forces is highly affected by time-dependent behavior of the superstructure (e.g., shortening and prestress losses) in addition to the effects of concrete relaxation in the columns. Although these forces are suspected to be reduced with time due to the beneficial effects of concrete relaxation, these effects are currently disregarded in the routine analysis of the columns of a CIP/PCBB, resulting in the overestimation of forces.

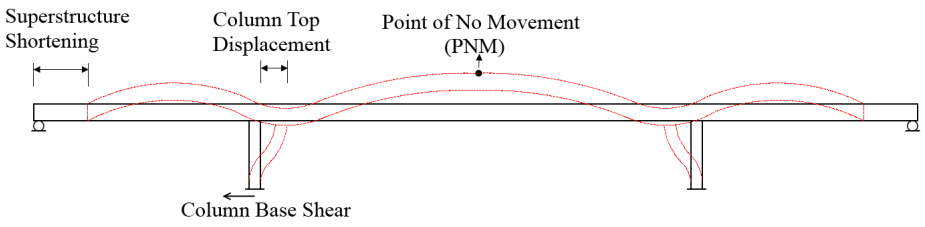

Fig. 1: Deformation of a posttensioned concrete box-girder bridge due to prestresing, creep, and shrinkage

Concrete is a structural material with time-dependent properties, such as shrinkage as well as creep and its associated stress relaxation, which significantly affect the structural behavior of prestressed bridges. On one hand, creep and shrinkage are unfavorable when the time dependent deformations cause loss of prestress and increase deflections, which may impair the serviceability of a structure. On the other hand, creep and its associated stress relaxation can be beneficial in the form of redistribution of stresses and reduction of stresses. Since creep and relaxation of concrete are different manifestations of the same viscoelastic material property, they have been used interchangeably in the literature. However, in this study, the relaxation term is used to refer to the loss of stress under a state of imposed constant strain and the creep term is used to refer to the increase in the strain under imposed sustained stress.

The effects of concrete creep and relaxation can be beneficial at two stages: (1) at early ages during hardening of concrete; and (2) long-term after maturity of concrete. The beneficial effects of concrete relaxation at early ages are mainly to reduce the restraint stresses induced by thermal dilation and autogenous shrinkage, thereby reducing the risk of cracking during hardening. In many cases, a reduction of restraint stresses by 30-40% due to stress relaxation in hardening concrete has been reported[1-3]. After maturity of concrete, the test data on a series of continuous reinforced concrete beams[4] and continuous prestressed concrete beams[5] subjected to a fixed displacement (settlement) verified the beneficial effects of relaxation by reducing the reaction forces with time. Moreover, Choudhury et al.[6] showed that considerable economy in design of reinforced concrete bridge columns subjected to imposed deformation can be achieved by including the beneficial effects of column creep due to the axial load. However, the beneficial role of concrete relaxation in reducing the deformation-induced forces in the columns of CIP/PCBB caused by time-dependent shortening of superstructure has not been examined.

Therefore, a systematic investigation is undertaken in this study to characterize concrete relaxation and demonstrate its beneficial effects on the design of the columns of a CIP/PCBB. To achieve the objective of the study, a combination of an experimental program and finite-element analysis (FEA) of a prototype CIP/PCBB was employed. The experimental program was used to characterize the concrete relaxation and subsequently establish suitable relaxation functions for concrete. Using these relaxation functions in the FEA, the variation of displacement-induced forces with time was calculated and compared to the elastic response. It is shown that concrete relaxation results in significant reduction of displacement-induced forces in the columns.

CONCRETE TIME-DEPENDENT PROPERTIES

The behavior of CIP/PCBB over time is dependent on the material properties. Creep/relaxation and shrinkage of concrete and steel relaxation are the most significant material properties affecting the long-term stresses and deformations of CIP/PCBB. The long-term prestress losses in prestressed concrete bridges occur due to the creep and shrinkage of concrete and the relaxation of prestressing steel.

Ignoring the thermal effects, the total strain of a prestressed concrete member at age, t, is typically comprised of the following: (1) stress-dependent strains (i.e., elastic and creep strains); (2) stress-independent strain (i.e., shrinkage strain), which can be expressed by Equation (1)[7].

(1)

where and is age of concrete when the initial stress is applied and when the strain is considered, respectively; is an indeterminate age between and ; is the initial stress applied at age ; is an elemental stress applied at age ; is the modulus of elasticity of concrete at age ; is the creep coefficient at time for loading at age ; and is the free shrinkage occurring between the ages and .

Using the principle of superposition [8], total creep strain at any time t is obtained as the sum of independent creep strains produced by stress changes at different ages with different duration of time up to t. Thus, creep strain at time t can be calculated using Equation (2).

(2)

where is the specific creep and can be calculated using Equation (3).

(3)

where is the creep function.

In order to discretize Equation (3), a total of n intervals are assumed, and it is also assumed that

the stress is invariant in each n time interval. Denoting time interval as $\Delta t_n = t_n - t_{n-1}$ and stress

increment as $\Delta\sigma_n = \sigma_n - \sigma_{n-1}$, the total creep strain can be defined by Equation (4).

(4)

with each creep strain increment from t_{n-1} to t_n being defined by Equation (5).

(5)

If the length of the member is maintained constant, will not change but the stress will gradually decrease because of creep. Using a unit step function for the history of stress-dependent strain, the history of stress is consequently represented by the relaxation function as expressed in Equations (6) and (7).

1 **(6)**

(7)

Bazant[9] showed that the exact solution presented in Equation (6) may be approximated by Equation (8) with 2% error between the exact and approximate solution.

(8)

where is the coefficient for age-independent correction and can be neglected except for *(*, where ; and the optimum value of can be found using Equation (9).

(9)

If the stress remains constant over time the relaxation function can be calculated directly from Equation (4), which yields to Equation (10).

(10)

The time-dependent properties are best obtained from results of tests conducted on specimens made of materials used in the actual structure and subjected to conditions similar to those to which the structure will be subjected. Owing to the long period of time required to obtain such test results, for each structure, reliable models for prediction of the aforementioned properties of concrete and prestressing steel are available in the literature. The most commonly used models are AASHTO LRFD 2010 Bridge Design Specifications[10], the CEB-FIP Mode1 Code[11], and the ACI Committee 92-209[12]. These models are suitable for incorporation into computer programs for the required analysis.

EXPERIMENTAL INVESTIGATION

SPECIMENS

Three different specimens were used to characterize the relaxation of the normal strength concrete over short durations (i.e., less than five days). The descriptions of these specimens are presented in Table 1. Two column specimens were used to quantify the relaxation under uniaxial compression at different loading ages, while a reinforced concrete (RC) beam was used to quantify the relaxation under flexure. Both columns were unreinforced with two different cross section sizes, allowing the size effect to be observed.

Table 1: Descriptions of the specimens used for the relaxation tests

Specimen number	Type	Diameter	Length	Loading ages (day)
1	Circular concrete column	203.2 mm (8 in.)	1.22 m (4 ft)	48, 76, 78, 84
2	Circular concrete column	304.8 mm (12 in.)	1.22 m (4 ft)	67
3	Circular RC beam	203.2 mm (8 in.)	1.22 m (4 ft)	130, 150

INSTRUMENTATION

To ensure that the specimens were subjected to a state of constant strain, strain gauges were used to monitor the changes in concrete/steel strains during concrete relaxation. For the column specimens, four surface mounted concrete gauges were attached in the four quadrants of the column outer surface at mid-height, as illustrated in Fig. 2. To ensure smooth, flat surfaces at the column ends to uniformly apply the axial load, they were capped with a thin layer of Hydro-Stone ® (i.e., 3.175 mm [0.125 in.] to 6.35 mm [0.25 in.]). For the RC beam, two concrete strain gauges were attached to the top and bottom surfaces (i.e., on the extreme compressive and tensile regions). In addition, the longitudinal and transverse steel reinforcement of the beam were instrumented with strain gauges to monitor the changes in the steel strain with time. A total of six strain gauges were attached to the steel spirals at Sections 1 and 2 to monitor changes in the transverse reinforcement, as illustrated in Fig. 3. Two of the six strain gauges were placed on the tension side while the remaining gauges were placed on the compression side. Instrumentation to monitor the longitudinal strains was similar to that of the spirals, where two of the six strain gauges were attached to the longitudinal bars on the tension side and the remaining gauges were attached to the longitudinal bars on the compression side at Sections 1 and 2, as illustrated in Fig. 3.

Each of the 12 steel strain gauges was labelled, as shown in the example below:

The first part describes whether the gauge was attached to the longitudinal reinforcement (L) or the transverse reinforcement (T). The second and the third parts identify the location of the gauge with respect to the position of the longitudinal and transverse reinforcement. The second part indicates the location of the nearest longitudinal bar to the gauge, while the third part determines the location of the nearest spiral to the gauge. The longitudinal bar numbers as well as the spiral numbers are indicated in Fig. 3.

In addition, to quantify thermal and shrinkage strains, stress-independent strains were monitored for an unloaded specimen located adjacent to the test specimen while the specimen was loaded.

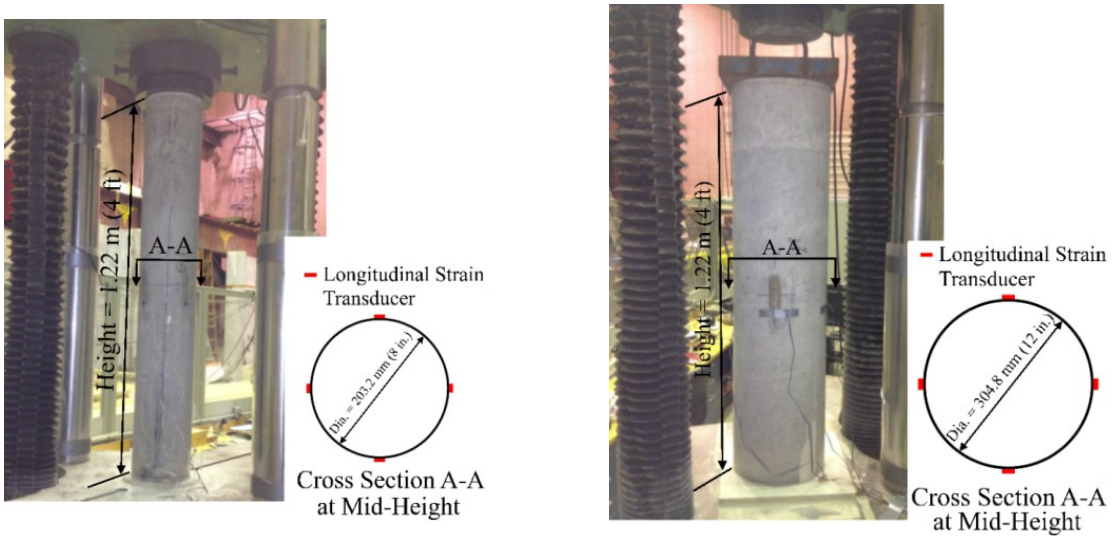

(a) 203.2 mm diameter specimen during test **(b) 304.8 mm diameter specimen before test**

Fig. 2: Instrumentation of concrete column specimens under axial compression

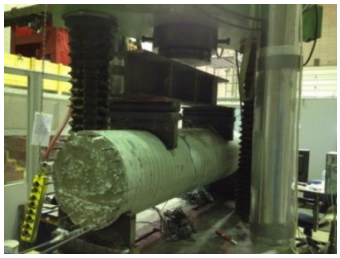

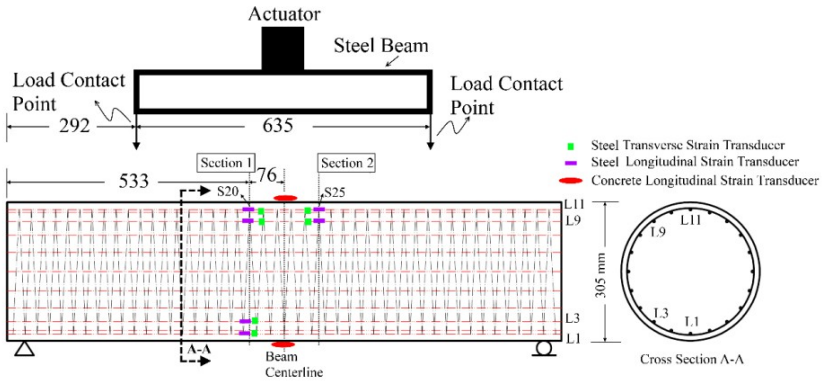

Fig. 3: Instrumentation of RC beam specimen under four-point bending (dimenstions are in mm)

TESTING APPARATUS AND METHODOLOGY

The SATEC uni-axial testing machine was used to perform the relaxation tests. The test unit included the hydraulic actuator and a data acquisition system. The SATEC machine was able to accommodate both the displacement and force control modes using the software provided with its data acquisition system. This software allows a test protocol to be defined by choosing the loading mode (displacement or force control mode), magnitude of the applied force or displacement, load rate, number of increments to apply the load, and test duration.

Initially, the specimens were loaded under a force control mode, in which the actuator displaced until the desired load was reached and the corresponding actuator displacement was recorded. Then, the machine was switched to a displacement control mode, where the previous recorded actuator displacement was applied to the specimen and held constant for the duration of test, simulating the state of constant strain.

LOADING

The three specimens were subjected to different states of constant strain, which included: (1) instantaneous axial compression; (2) incremental axial compression; and (3) instantaneous flexure. Using the three specimens and the three loading protocols, a total of seven tests at different concrete ages were performed. The details of these tests are summarized in Tests 1 through 3 were performed using the first loading protocol, in which an elastic strain was applied and maintained over the entire duration of the test. Tests 4 and 5 were performed using the second loading protocol, in which the uni-axial compression was incrementally applied to the column specimen through a number of time-steps over the duration of the test. At the beginning of each time step, the specimen was subjected to an elastic strain which was held constant until the beginning of the next time-step, when the strain was increased. This procedure was repeated for all the time steps. The cumulative strain at the end of the time-steps was less than the elastic strain threshold. Test 4 consisted of 12 ten-hour time-steps, while six 15-hour time-steps were used for Test 5. .

Tests 1 through 3 were performed using the first loading protocol, in which an elastic strain was applied and maintained over the entire duration of the test. Tests 4 and 5 were performed using the second loading protocol, in which the uni-axial compression was incrementally applied to the column specimen through a number of time-steps over the duration of the test. At the beginning of each time step, the specimen was subjected to an elastic strain which was held constant until

the beginning of the next time-step, when the strain was increased. This procedure was repeated for all the time steps. The cumulative strain at the end of the time-steps was less than the elastic strain threshold. Test 4 consisted of 12 ten-hour time-steps, while six 15-hour time-steps were used for Test 5.

Table 2: Details of the seven relaxation tests

Test Number	Specimen used	Specimen age at loading (day)	Test duration (hours)	Loading protocol	Initial strain (με)
1	1	48	109	Instantaneous axial compression	422
2	2	67	112	Instantaneous axial compression	452
3	1	76	73	Instantaneous axial compression	435
4	1	78	116	Incremental axial compression	43*
5	1	84	90	Incremental axial compression	87*
6	3	130	119	Instantaneous flexure- precracking	198
7	3	150	120	Instantaneous flexure- postcracking	682

*The mean applied strain for all the time steps

Tests 6 and 7 were performed on RCCB subjected to the third loading protocol using four-point bending. For Test 6, the specimen was loaded under constant flexural strain prior to the unit experiencing any flexural cracks. For Test 7, the load was applied to cause flexural cracks on the tension side, and then a constant flexural strain was applied and maintained. Soon after the completion of Test 7 (i.e., within half an hour) and the beam was unloaded, it was monotonically loaded under displacement control until failure. This was carried out to evaluate any impact of the relaxation test on the flexural behavior of the beam.

OBSERVED BEHAVIOR

Variations in concrete strains and stresses with time recorded for the seven tests are shown in Fig. 4. In general, the concrete strain remained constant while the stress decreased with time for all the tests. Additionally, the variations in strain and stress and corresponding relaxation were quantified at the end of each test, as given in Table 3. For all the tests, the shrinkage and thermal (stress-independent) strains were found to be less than 10 με, and were consequently considered negligible. The applied (stress-dependent) strain varied slightly with the time (i.e., ±22 με) during all the tests, except for Test 7, where the highest variation of ±57 με was observed.

(a) Concrete strain variation vs. time **(b) Concrete stress variation vs. time**

Fig. 4: Test results

For the identical specimen sizes with similar initial axial compressive stresses, Test 1 resulted in 49% stress relaxation, while Test 3 which was loaded 28 days later than Test 1, exhibited 39% reduction in stress. Moreover, the size effect can be observed by comparing the results from Test 2 to Test 3, which had two different cross section sizes but similar applied stresses and loading ages. The results indicated that after 72.5 hours the axial stress for the larger specimen used for Test 2 decreased from the initial stress by 32%, while the corresponding reduction was 41% for the smaller specimen used in Test 3. For Tests 4 and 5, the concrete stress after 90 hours was reduced by 14.5% and 20.5%, respectively, as the concrete strain remained constant. Since the loading age and specimen size were similar for the two tests, the larger reduction in stress for

Test 5 relative to Test 4 is attributable to the higher stress applied to a fewer time steps for Test 5 than Test 4.

For Test 6, the reduction in the concrete stress at the end of the test was 20.4%. The concrete compressive strain did not change with time while the compressive stress was reduced by 14.6% at the end of Test 7. The strain gages placed on the tension side indicated cracking of the specimen.

Fig. 5 shows the variation of strain in the steel longitudinal and transverse reinforcements with time for Tests 6 and 7. For Test 6, the longitudinal strains were below yielding strain and the variation of strain in longitudinal reinforcement was insignificant. For the transverse reinforcement, most of the strain gages recorded zero strain which was expected since the beam was under pure flexure at the mid-span. However, two of the strain gages showed strain as high as 100 με which could be attributed to the possible misalignment of the gages.

(a) Test 6 **(b) Test 7**

Fig. 5: Variation of strains in steel longitudinal and transverse reinforcement with time

For Test 7, the tensile longitudinal strains show the yielding of the steel and slight strain variation with time. Similar to Test 6, the recorded transverse strains were zero, except for one strain gage which showed a strain as high as 200 με. This is most likely due to the local micro cracks at the location of the gage.

Table 3: Results of the seven relaxation tests

Test	Variation in mean applied strain (με)	Thermal and shrinkage strains (με)	Stress (MPa)		Stress relaxation (%)
			Start	End	
1	±6	< 10	13.7	7.0	49
2	±11	< 10	13.9	9.0	35
3	±22	< 10	14.3	8.7	39
4	±5	< 10	15.2	11.9	22
5	±4	< 10	15.0	11.9	21
6	±10	< 10	4.6	3.7	21
7	±57	< 10	17.2	14.5	16

CONCRETE RELAXATION FUNCTIONS

The relaxation function was established to determine the reduction in the stress due to a unit constant strain based on the test results reported above and the analytical creep models. For the analytical models, a combination of the time step method based on FEA and a simplified analysis using Equations (8) and (10) were employed to estimate the relaxation function corresponding to each test. Accordingly, a creep coefficient was estimated for each case as a function of time using the AASHTO LRFD Bridge Design Specification 2010[10] prediction models. Except the loading age, the other parameters used in the AASHTO models, including the concrete compressive strength and humidity were calibrated for the first test such that the best agreement was found between the estimated and measured relaxation functions.

Using the Midas Civil software[13], the FEA was performed with due consideration to specimen geometry, creep, and loading protocol. A constant strain was applied to the FEA model such that the corresponding initial stress was the same as the measured initial stress for the test. This was achieved by adjusting the concrete modulus of elasticity. The same calibrated values for concrete

compressive strength and humidity were used to estimate creep and shrinkage in the analytical models developed for the remaining tests. Fig. 6 and Fig. 7 show the comparison between the calculated relaxation functions based on the test results and the different analytical models for the concrete column and RC beam specimens, respectively. In Fig. 6, the simplified analysis and the Bazant's method produced identical curves.

(a) Test 1 **(b) Test 2**

(c) Test 3 **(d) Test 4**

(e) Test 5

Fig. 6: Concrete relaxation functions for the compressive stress of column specimens calculated using the different methods

(a) Test 6 **(b) Test 7**

Fig. 7: Concrete relaxation functions for the compressive stress of RC beam specimen calculated using the FEA

In general, a good agreement is found between the test results and the FEA results for the different tests. The simplified analysis and the Bazant's method resulted in identical approximation of the relaxation functions for the different tests due to the short duration of the tests (i.e., less than 5 days). The relaxation functions estimated by the simplified analysis and Bazant's method did not correlate well with the test results for the first 48 hours of Tests 1 through 5. After 48 hours, it is observed that the simplified analysis and Bazant's method resulted in the overestimation of the relaxation functions for Tests 1 and 2, while underestimated the relaxation functions for Tests 4 and 5.

PROTOTYPE BRIDGE

The Floodway Viaduct Bridge, constructed in California, was used to demonstrate the interrelated time-dependent effects of concrete on a CIP/PCBB. The Floodway Viaduct Bridge is a curved CIP/PCBB, is 1829.12 m (6001 ft) long, and consists of 33 spans distributed among 8 different isolated frames. For this study, Frame 6 of the bridge, the longest frame, was selected for the analytical investigation. Using the FEA of the bridge, the effects of concrete creep/relaxation and shrinkage on the shortening of superstructure and subsequently on the displacement-induced forces in the columns were investigated.

DESCRIPTIONS OF FRAME 6

Frame 6 of the Floodway Viaduct Bridge is 258.8 m (849 ft) long and consists of 4 spans, as shown in Fig. 8. In addition, the box-girder cross section of Frame 6 is shown in Fig. 8, where the box-girder's height remains constant over the entire frame length. However, at the bents and the abutments, the stem and the soffit of the box-girders were flared over a short length to withhold the stress concentration.

The material properties used for the posttensioned box-girder, deck, and reinforced concrete in the columns are presented in Table 4 Moreover, presents the posttensioning details of Frame 6. The details in regard to the application of prestressing force, including the size and location of the prestressing tendons, amount of prestessing force per girder, and the duct size were not included in the plans. Hence, these details were left to the contractor to decide upon with the engineer's approval per AASHTO LRFD Design Specifications (2010) recommendations.

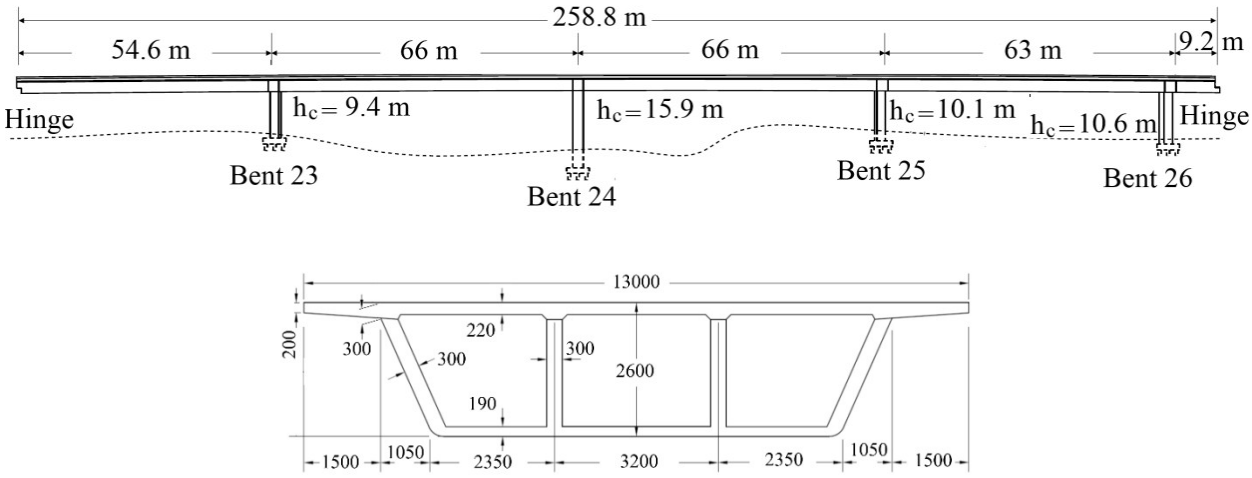

Fig. 8: Elevation view and cross sectional view (mm) of Frame 6

Table 4: Material properties of Frame 6

Box-girder/deck			Reinforced concrete	
(MPa)	(MPa)	F_u (MPa)	f_y (MPa)	(MPa)
28	35	1862	420	25

Note: : release compressive strength; *:* 28-day compressive strength; F_u: ultimate strength of prestressing tendons; f_y: yield strength of reinforcing streel.

Table 5: Prestressing details of Frame 6

Jacking force (kN)	Initial axial stress (MPa)	Anchorage set (mm)	Friction coefficient, μ	Wobble coefficient, κ (1/m.)
49200	6.7	10	0.2	0.000656

FINITE-ELEMENT ANALYSIS

The FEA of the bridge was performed using the Midas Civil software[13] based on the construction stage analysis and time-step method to analyze time-dependent stresses and deformations. Beam elements were used to model the box-girder and the columns of Frame 6. The significant parameters affecting time-dependent behavior of CIP/PCBB, including concrete creep/relaxation and shrinkage, prestress losses, support locations, and construction stages were taken into account in the FEA.

MODEL ASSUMPTIONS

The following assumptions were used in the FEA of the bridge to avoid unnecessary complications:

The bridge was modeled with zero curvature in the horizontal plane.
Bridge box-girder remained elastic and uncracked when the time-dependent deformations were imposed.
The restraining effects of box-girder nonprestressed reinforcement on shrinkage were disregarded.
The loads acting on the bridge frame were dead load and prestressing force.
Linear elastic behavior was used for columns, although the stiffness was modified to reflect the effective stiffness in the case of cracking using moment-curvature analysis.

CONSTRUCTION STAGES

The construction of each frame of a CIP/PCBB in California typically involves the following stages: (1) construction of the foundation (i.e., cast-in-place drilled H-piles [CIDH], or pipe piles); (2) construction of piers; (3) construction of soffit and stem of the box-girder on shoring; (4) construction of the deck; (5) application of prestressing force, (6) removal of shoring; and (7) construction of barriers followed by the service conditions. These seven construction stages were simulated in the FEA to reflect the most common practice used for the construction of CIP/PCBB in the state of California, as shown by the timetable in Fig. 9. The construction stages of Frame 6 modeled in the Midas Civil software[13] are illustrated in Fig. 10. It can be inferred from the construction stages that the columns were approximately 180 days of age when they were subjected to the lateral deformation imposed by the box-girder. Additionally, as soon as the concrete shrinkage begins in an indeterminate bridge frame (i.e., the box-girder before the deck cast), tensile creep deformation is produced which indeed alleviates the shrinkage deformation. Assuming an age of seven days at the beginning of shrinkage resulted in a loading age of seven days for the creep initiation in the box-girder. Consequently, the loading ages of seven and 180 days were used in the estimation of the creep coefficients for the box-girder and the columns, respectively.

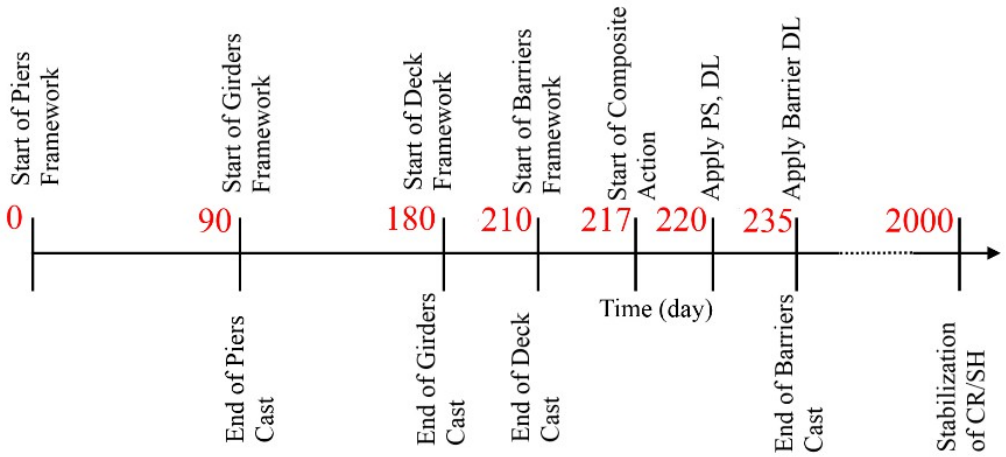

Fig. 9: Timetable used for construction stages of Frame 6

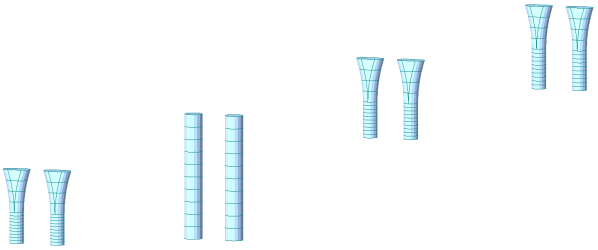

(a) Constructed piers

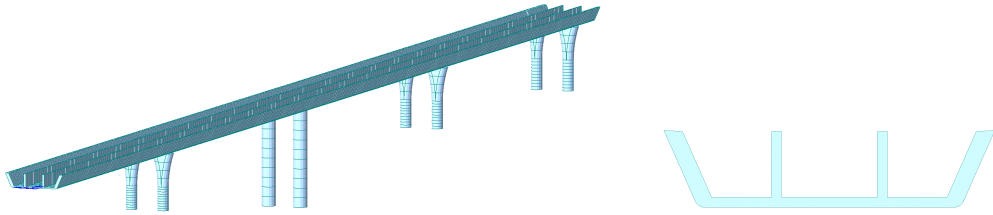

(b) Constructed box-girder

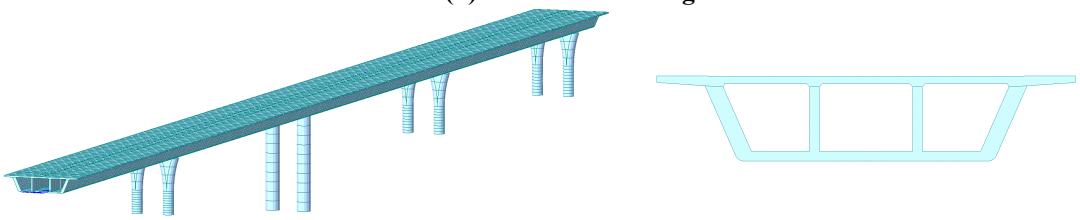

(c) Constructed deck

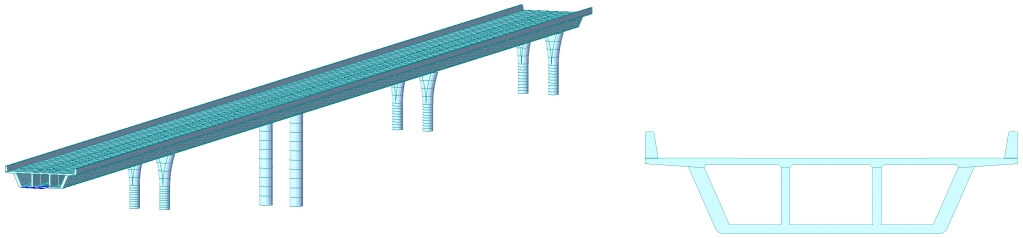

(d) Constructed barriers

Fig. 10: Construction stages of Frame 6 simulated in the FEA

MATERIAL MODELS

Table 6 presents the models used to calculate the material properties in the FEA. The variation of compressive strength with time was disregarded for the columns, and the column modulus of elasticity was calculated using the AASHTO LRFD Bridge Design Specifications[10] model based on the 28-day compressive strength after which the additional gain in modulus of elasticity was negligible. This is a valid assumption, since the columns were at least three months old by the time the box-girder was cast and the time-dependent deformations were imposed on the columns. For the box-girder, the variation of concrete compressive strength with time was estimated using ACI[12].

Due to the different concrete compressive strengths of the box-girders and columns and different volume to surface ratio, two separate creep and shrinkage models were employed for the columns and box-girders.

The compressive strengths provided in Table 4, the assumption of 60% for the relative humidity, and the age of 7 days for the beginning of shrinkage were used to estimate the creep and shrinkage deformations based on AASHTO LRFD Bridge Design Specifications[10]. In addition, the loading ages of seven and 180 days were assumed for the box-girders and the columns, respectively, to calculate the creep coefficient.

Table 6: Prediction models for the material properties

Material property	Model	
	Box-girder	Column
Variation in concrete compressive strength with time	ACI	Not Applicable
Modulus of elasticity	AASHTO	AASHTO
Concrete creep/relaxation	AASHTO	AASHTO
Concrete shrinkage	AASHTO	AASHTO
Relaxation of posttensioned tendons	AASHTO	Not Applicable

LOADING

Two load cases including the dead load and the prestessing force were imposed on CIP/PCBB. According to the construction stages, the prestressing force was applied 40 days after completion of the deck cast. Following the application of the prestessing force, the falsework was removed which was simulated in the analytical models by activation of the dead load of the bridge. The total prestessing force was equally distributed among the girders and was applied to each girder by placing a tendon in the middle of the girder. The size of each tendon was chosen such that the geometry constraints were satisfied and the stress in each tendon was below the yielding strength of the tendons. Based on the diameter of the tendons, the appropriate duct size was included in

the model. In addition, the tendons were modeled as bonded tendons with perfect bonding to the concrete. Thus, the box-girder section properties used in the analyses reflected the transformed section properties.

COLUMN EFFECTIVE STIFFNESS

Moment-curvature analysis was performed using the XSection software to determine the cracking potential in the columns due to the displacement-induced forces. The required axial force for the moment-curvature analysis was estimated using the FEA of the bridge when the bridge was subjected only to the dead load. The FEA was initially completed assuming the columns remained uncracked (i.e., gross section properties) and then the resulting column moments were compared to the column cracking moments calculated using the XSection software. When the column was cracked, the effective stiffness calculated by the moment-curvature analysis was used in the FEA to account for cracking. This was accomplished by decreasing the column gross moment of inertia in the FEA using a reduction factor. The reduction factor was calculated as the ratio of the effective to gross stiffness. Subsequently, the column moments were reevaluated and compared to the cracking moment to verify the appropriate use of the column stiffness. The mean reduction factor was found to be 0.52 for the four columns.

ANALYTICAL RESULTS

The FEA results for the time-dependent effects on the box-girder and the columns are demonstrated in this section. The effects of concrete relaxation are integrated in the FEA results by showing the response of the bridge with and without column relaxation. For the box-girder, the changes in shortening strain of box-girder with time are evaluated. For the columns, the changes in the top lateral displacement and the corresponding base shear force with time are evaluated. As an example, Fig. 11 shows the deformed shape of the bridge predicted by the FEA due to prestressing, creep, and shrinkage after 2000 days from completion of piers construction.

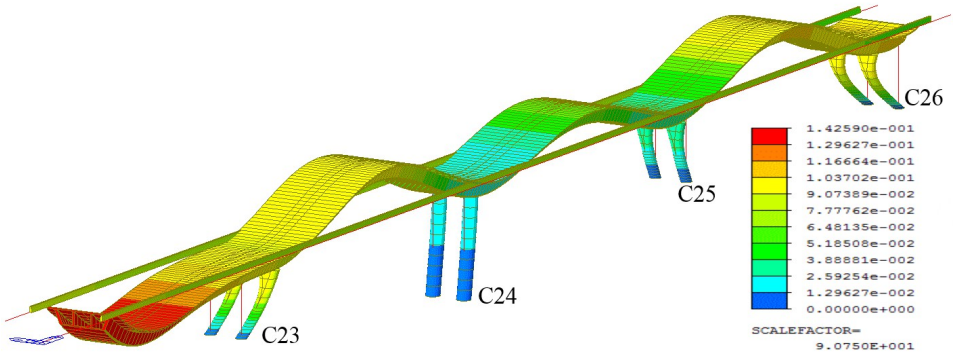

Fig. 11: Deformed shape of Frame 6 (m) predicted by the FEA due to presterssing, creep, and shrinkage after 2000 days from completion of piers construction

SHORTENING STRAIN RATE OF THE SUPERSTRUCTURE

The shortening strain rate of the superstructure was calculated as the difference between the displacements at the two ends of the bridge divided by the length of the bridge. Fig. 12 shows the

shortening strain rate of the box-girder due to dead load, prestress, creep, and shrinkage components in addition to the summation of these components. It may be observed the total shortening strain rate is dominantly affected by the shrinkage component. After 2000 days, the total shortening strain rate is comprised of 68.8%, 16.6%, 20.1%, and -5.6% due to shrinkage, creep, prestress, and dead load, respectively. Though small, the dead load causes opposite direction strains to that due to creep, shrinkage, and post-tensioning, as its effect lengthen the bridge. Since the superstructure is significantly stiffer than the columns, the column creep had negligible effect on the shortening of the superstructure, as shown in Fig. 12.

Fig. 12: Shortening strain rate of the superstructure calculated using the FEA with column relaxation (single line) and without column relaxation (double line)

COLUMN TOP LATERAL DISPLACEMENT

Fig. 13 shows the results for the column top lateral displacement due to dead load, prestress, creep, and shrinkage components in addition to the summation of these components for C25 and C26. The shrinkage of the superstructure has the largest contribution to the column displacement compared to the other components. After 2000 days, for C26, the total displacement is comprised of 59.3%, 22.2%, 14.5%, and 4% due to shrinkage, creep, prestress, and dead load, respectively. Typically, the further a column is from the point of no movement (PNM), the larger lateral displacement due to the superstructure shortening is imposed on the column. Accordingly, the displacement of the two exterior columns (i.e., C23 and C26) was significantly greater than that of the two interior columns (i.e., C24 and C25). The largest top of column displacement was 103 mm (4.1 in.) and belonged to C26, while C24 had the smallest displacement of 23 mm (0.9 in.).

(a) C25 **(b) C26**

(c) C26 – the first 90 days

Fig. 13: Variation of column lateral top displacements with time calculated using the FEA with column relaxation (single line) and without column relaxation (double line)

COLUMN BASE SHEAR FORCE

The contribution of the different components including dead load, prestress, creep, and shrinkage to the total base shear force was evaluated, as presented in Fig. 14. In agreement with displacements and strain rates, the shrinkage of the superstructure affected the base shear force more than the other components. After 2000 days, for C26, the total base shear force is comprised of 125.5%, -82.6%, 44.0%, and 13.1% due to shrinkage, creep (in column), prestress, and dead load, respectively. As shown in Fig. 14, the secondary effect of creep acted in the opposite direction to the dead load as well as the secondary effects of pretstress and shrinkage. Moreover, the column creep significantly reduced the deformation-induced forces in the column as seen in Fig. 14. The reduction in the column base shear force in C23 was 42.3% after 2000 days due to column relaxation. In general, the higher the column displacement was, the more shear force was induced at the column base. Thus, similar to the column displacement, the two exterior columns (i.e., C23 and C26) were subjected to significantly higher base shear forces than the two interior columns (i.e., C24 and C25). The maximum estimated column base shear

force was -1819 kN (-409 kips) and occurred in C23, while C24 experienced much smaller shear force (i.e., -89 kN [-20 kips]).

Using the FEA results for the base shear force, the variation in the column moment with time was calculated and then compared to the results of the moment-curvature analysis. Based on the moment-curvature analysis, all the columns cracked due to the time-dependent effects except C24, which is located the nearest to the PNM. Additionally, the calculated moment by the FEA is less that the yielding moment of column estimated by the moment-curvature analysis for all of the columns. This would not be true if the beneficial effects of concrete relaxation were not considered.

(a) C25 **(b) C26**

(c) C26 - the first 90 days

Fig. 14: Variation of column base shear force with time calculated using the FEA with column relaxation (single line) and without column relaxation (double line)

SUMMARY AND CONCLUSIONS

A combination of an experimental study and the FEA was used in this paper to first characterize concrete relaxation and subsequently demonstrate the beneficial effects of relaxation on displacement-induced column forces of a CIP/PCBB. Three different specimens were used to characterize the relaxation of the normal strength concrete over short durations (i.e., less than five days) after the concrete had fully matured (i.e., after 28 days). The three specimens were subjected to a state of constant strain using three different loading protocols including: (1) instantaneous axial compression; (2) incremental axial compression; and (3) instantaneous flexure. Loading protocols 1 and 2 were performed on concrete column specimens of two different cross section sizes, while the third loading protocol was performed on the reinforced concrete (RC) beam. Using the three specimens and the three loading protocol, a total of seven tests at different loading ages was performed, which led to the following conclusions:

In all tests, the beneficial effects of concrete relaxation on the displacement-induced forces/stresses were observed by reducing concrete forces/stresses with time under the state of a constant strain. The most significant portion of the reduction of the stress occurred within the first 48 hours of the tests.

Similar to creep, the relaxation was appreciably affected by the age of loading and the magnitude of the initial applied load. Hence, Test 1 with the smallest loading age resulted in the largest relaxation (i.e., 49% reduction in stress after 109 hours) among the seven tests.

By incrementally applying the constant displacement in Tests 4 and 5, a more realistic loading expected on columns supporting the PCBBs was simulated, for which the beneficial effects of relaxation were still significant in reducing the stresses.

Conducting the relaxation tests on the RC beam indicated that the relaxation was not affected by the cracking of the specimen except that the magnitude of stresses and strains in concrete and steel increased due to cracking.

The relaxation function calculated by the FEM led to a better agreement with the test results

compared to the approximate method proposed by Bazant[9] and the simplified analysis. By applying these functions in the FEM of CIP/PCBB, column forces can be accurately calculated with due consideration to the effects of concrete relaxation.

The FEA of the demonstrative CIP/PCBB was performed using the Midas Civil software[13] to analyze time-dependent stresses and deformations over numerous time-steps from the time of construction to the completion of the CIP/PCBB with due consideration to concrete relaxation. The significant parameters affecting time-dependent behavior of CIP/PCBB, including concrete creep/relaxation and shrinkage, prestress losses, support locations, column effective stiffness, and construction stages were taken into account in the FEA. The beneficial effects of concrete relaxation were demonstrated by comparing the results when the CIP/PCBB was analyzed with the relaxation functions for the columns with the corresponding results without relaxation functions for the columns. Based on the findings of the FEA, the following conclusions were drawn:

The shrinkage of the CIP/PCBB superstructure had a significantly larger contribution to the shortening strain rate of superstructure, column top lateral displacement, and the corresponding base shear force compared to the corresponding effects of dead load, prestress, and creep.
Based on the moment-curvature analysis, the exterior columns would crack due to displacement-induced forces, while the column adjacent to the PNM remained uncracked.
Due to the column relaxation, the ultimate base shear force was reduced by as much as 53% for the exterior column (i.e., C26).

REFERENCES

1. Bosnjak, D., "Self-Induced Cracking Problems in Hardening Concrete Structure," PhD dissertation, Department of Structural Engineering, NTNU, Trondheim, Norway, 2001.
2. Atrushi, D. S., "Tensile and Compressive Creep at Early Age Concrete: Testing and Modeling," Department of Structural Engineering, the Norwegian University of Science and Technology (NTNU), Trondheim, Norway, 2003.
3. Schutter, G. D., "Applicability of Degree of Hydration and Maturity Method for Thermo-Viso-Elastic Behavior of Early Age Concrete," Cement & Concrete Composite, V. 26, No. 5, 2004, pp. 437-443.
4. Ghali, A., Digler, W., Neville, A. M., "Time-Dependent Forces Induced By Settlement of Supports in Continuous Reinforced Concrete Beams," *ACI Structural Journal*, V. 66, No. 11, 1969, pp. 907-915.
5. Digler, W., Ghali, A., Kountouris, C., "Time-Dependent Forces Induced By Settlement in Continuous Prestressed Concrete Structures," *ACI Structural Journal*, V. 80, No. 12, 1970, pp. 507-515.
6. Choudhury, D., Mari, A. R., Scordelis, A. C., "Design Of Reinforced Concrete Bridge Columns Subjected To Imposed Deformations," *ACI Structural Journal*, V. 85, No. 5, 1988, pp. 521-529.
7. Ghali, A., Favre, R., Elbadry, M., "Concrete Structures- Stresses and Deformation," *Spon Press*, 2002.
8. McHenry, D., "A New Aspect of Creep in Concrete and Its Application to Design," *Proc. ASTM,* V. 43, 1943, pp. 1069-84.
9. Bazant, Z. P., Kim, S., "Approximate Relaxation Function for Concrete," *Journal of the Structural Division,* V. 105, No. 12, 1979, pp. 2695-2705.
10. American Association of State Highway and Transportation officials, "AASHTO LRFD Bridge Design Specifications," Washington, DC, 2010.
11. Comite Euro- International du Beton, Bulletin d'information, CEB-FIP, "Evaluation of Time Dependent Behavior of Concrete," Paris, France, 1990.
12. ACI Committee 318, "Building Code Requirements For Structural Concrete And Commentary," Farmington Hills, MI, 2011.
13. MIDAS Civil Software, "Analysis Reference." 2013.